JNeurosci
THE JOURNAL OF NEUROSCIENCE

Research Articles: Cellular/Molecular

Opioid Receptors Modulate Firing and Synaptic Transmission in the Paraventricular Nucleus of the Thalamus

https://doi.org/10.1523/JNEUROSCI.1766-22.2023

Cite as: J. Neurosci 2023; 10.1523/JNEUROSCI.1766-22.2023

Received: 15 September 2022
Revised: 24 February 2023
Accepted: 1 March 2023

Opioid Receptors Modulate Firing and Synaptic Transmission in the Paraventricular Nucleus of the Thalamus

Guoqiang Hou [1,2,3], Shaolei Jiang [1,4], Gaowei Chen [1,2,3,5], Xiaofei Deng [1,2,3], Fengling Li [1,2,3], Hua Xu [1,2,3], Bo Chen [1,2,3,5], Yingjie Zhu [1,2,3,5,6,7,*]

[1] Shenzhen Key Laboratory of Drug Addiction, Shenzhen Neher Neural Plasticity Laboratory, the Brain Cognition and Brain Disease Institute, Shenzhen Institute of Advanced Technology, Chinese Academy of Sciences, Shenzhen, 518055, China.
[2] Shenzhen-Hong Kong Institute of Brain Science-Shenzhen Fundamental Research Institutions, Shenzhen, 518055, China.
[3] Faculty of Life and Health Sciences, Shenzhen Institute of Advanced Technology, Chinese Academy of Sciences, Shenzhen, 518055, China.
[4] University of Shanghai for Science and Technology, Shanghai, 200093, China.
[5] University of Chinese Academy of Sciences, Beijing, 100049, China.
[6] CAS Center for Excellence in Brain Science and Intelligence Technology, Chinese Academy of Sciences, Shanghai, 200031, China.
[7] CAS Key Laboratory of Brain Connectome and Manipulation, the Brain Cognition and Brain Disease Institute (BCBDI), Shenzhen Institute of Advanced Technology (SIAT), Chinese Academy of Sciences, Shenzhen, 518055, China.
*Correspondence: yj.zhu1@siat.ac.cn (Y.Z.)

Abbreviated title: Opioid Receptors Modulate Firing and Synaptic Transmission in PVT

Number of pages (44)
Number of figures (7), tables (0), multimedia (0), and 3D models (0)
Number of words for abstract (122), introduction (634), and discussion (992)

Acknowledgements

We thank Dr. Ming-Hu Han and Dr. Jianyuan Sun for comments on the manuscript. This work was supported by Science and Technology Innovation 2030 - Major Project (2021ZD0202103); National Natural Science Foundation of China (31900809, 81922024, 82171492); China Postdoctoral Science Foundation Grant (2019M653116); Science, Technology and Innovation Commission of Shenzhen Municipality (RCJC20200714114556103, ZDSYS20190902093601675 and JCYJ20210324141201003); Guangdong Basic and Applied Basic Research Foundation (2021A1515010729); Guangdong Provincial Key Laboratory of Brain Connectome and Behavior (2017B030301017).

Author contributions

Y.Z. conceived this study and designed the experiments. G.H. and S.J. conducted patch clamp recording, immunostaining experiments and analyzed data. G.H., H.X., X.D., F.L., G.C., and B.C. conducted stereotaxic surgery, retrograde tracing and single-cell RT PCR experiments. G.H. and Y.Z. wrote the manuscript.

Conflict of interests

The authors declare no competing financial interests.

Abstract

The paraventricular nucleus of the thalamus (PVT) is involved in drug addiction-related behaviors, and morphine is a widely used opioid for the relief of severe pain. Morphine acts through opioid receptors, but the function of opioid receptors in the PVT has not been fully elucidated. Here, we used *in vitro* electrophysiology to study neuronal activity and synaptic transmission in the PVT of male and female mice. Activation of opioid receptors suppresses the firing and inhibitory synaptic transmission of PVT neurons in brain slices. On the other hand, the involvement of opioid modulation is reduced after chronic morphine exposure, probably due to desensitization and internalization of opioid receptors in the PVT. Overall, the opioid system is essential for the modulation of PVT activities.

Key words: opioid receptor, paraventricular nucleus of the thalamus, PVT, zona incerta, firing, synaptic transmission, chronic morphine exposure

Significance statement: Opioid receptors modulate the activities and synaptic transmission in the PVT by suppressing the firing rate and inhibitory synaptic inputs. These modulations were largely diminished after chronic morphine exposure.

Introduction

The paraventricular nucleus of the thalamus (PVT) is a part of the dorsal midline thalamus (dMT) and acts as a central hub that integrates cortical and subcortical inputs to regulate diverse behavioral responses (Kirouac, 2015; Millan et al., 2017). The PVT has diverse connections with many nuclei, including the hypothalamus, hippocampus, amygdala, and prelimbic cortex, and sends large projections to other regions involved in motivation and behavior regulation, such as the nucleus accumbens. While the efferent projections are primarily glutamatergic, receptors for several neuromodulators and neuropeptides can be found in the PVT neurons, including serotonin, dopamine, norepinephrine, corticotropin-releasing hormone, orexin, and endogenous opioids (Kirouac, 2015; Barson et al., 2020). Studies have implicated the PVT in circadian rhythm, acute and chronic stress regulation, drug addiction-related behavior, attention processing, and decision-making (Iglesias and Flagel, 2021; Flagel, 2022).

Recently, the PVT has been identified as a key node in the neural circuits of drug addiction (Zhou and Zhu, 2019; Zhou et al., 2021). The PVT can be activated by acute exposure to cocaine, amphetamine and morphine (Deutch et al., 1998; Zhu et al., 2016). PVT neurons projecting to the nucleus accumbens (NAc) shell are recruited during spontaneous or naloxone-precipitated morphine withdrawal. PVT mediates aversion and morphine-associated memories. Activation of the PVT→NAc pathway drives aversion in morphine withdrawal-induced conditioned place aversion (CPA)

tests (Zhu et al., 2016; Do-Monte et al., 2017; Keyes et al., 2020). Furthermore, the PVT→NAc pathway is both sufficient and necessary to drive aversion and heroin seeking following abstinence but not extinction (Giannotti et al., 2021). These findings are consistent with recent studies proposing that PVT neurons encode the salience of behaviorally relevant stimuli (Zhu et al., 2018; Choi et al., 2019), a proposal that suggests the PVT plays a fundamental role in behavioral control (Zhou and Zhu, 2019).

Opioids, such as morphine, are clinically effective analgesics, but they also induce euphoria and adaptive changes in reward circuits (Le Merrer et al., 2009). Morphine acts through G protein-coupled opioid receptors to modulate presynaptic and postsynaptic ion channels (Luscher and Slesinger, 2010; Nockemann et al., 2013) and disinhibit inhibitory control to modulate pain and reward (Zhang et al., 2014; Baimel and Borgland, 2015). Opioid receptors comprise three homologous G protein-coupled receptors (GPCRs) known as mu- (μ), delta- (δ) and kappa- (κ) opioid receptors (MORs, DORs and KORs, respectively). Activation of opioid receptors inhibits neurons by activating inwardly rectifying potassium currents (Minami and Satoh, 1995; Brunton and Charpak, 1998; Ikeda et al., 2000), and opioid receptors are activated by endogenous opioid peptides under physiological conditions (Darcq and Kieffer, 2018). In addition, high expression of MOR and KOR has been found in midline thalamic nuclei, particularly the PVT (George et al., 1994; Mansour et al., 1994). The μ-opioid system in midline thalamic nuclei may be involved in

ameliorating aversive or defensive behavioral states associated with stress, withdrawal, physical pain or social rejection (Goedecke et al., 2019) and indeed modulates defense strategies against a conditioned fear stimulus in male mice (Bengoetxea et al., 2020). Intra-PVT infusion of a KOR agonist inhibits drug-seeking behavior (Marchant et al., 2010). KOR activation inhibits anterior PVT (aPVT) neurons in mice at different ages, particularly around puberty, suggesting a possible role for KOR in regulating aPVT-related brain functions, including the stress response and drug-seeking behavior, during adolescence (Chen et al., 2015). However, to date, it remains unclear how morphine affects the activity of PVT neurons and whether chronic morphine exposure alters this modulation.

In this study, we used patch clamp recording to test the effects of morphine and opioid receptor agonists on the activities of PVT neurons and synaptic inputs to the PVT. We also examined the functions of opioid receptors in the PVT after chronic morphine treatment. Taken together, this study illustrates the modulatory role of opioids in the activities of PVT neurons.

Materials and Methods

Subjects

Male and female mice aged 8-12 weeks were used in the experiments. Mice were maintained at 22-25 °C under a 12-hour light-dark cycle. All animal husbandry and experimental procedures in this study were approved by the Animal Care and Use

Committees at the Shenzhen Institute of Advanced Technology (SIAT), Chinese Academy of Sciences (CAS). C57BL/6 mice were obtained from Charles River Laboratories in Beijing and Hangzhou, China. GAD2-Cre (JAX stock number: 010802) were used in the current study.

Drugs

APV, CNQX, picrotoxin, DAMGO, naloxone, U50488, SNC80 and Tertiapin-Q were purchased from Tocris Bioscience.

Electrophysiological recording

Procedures to prepare acute brain slices and perform whole-cell recordings with optogenetic stimulation were similar to those described previously (Zhu et al., 2016). Briefly, mice were anesthetized with isoflurane and decapitated in the morning (light cycle). Brains were rapidly dissected and coronal slices of 250-300 μm containing the PVT were prepared using a vibratome (VT-1000S, Leica) in an ice-cold choline-based solution containing (in mM) 110 choline chloride, 2.5 KCl, 0.5 $CaCl_2$, 7 $MgCl_2$, 1.3 NaH_2PO_4, 1.3 Na-ascorbate, 0.6 Na-pyruvate, 25 glucose and 25 $NaHCO_3$, saturated with 95% O_2 and 5% CO_2. Slices were incubated in 36 °C oxygenated artificial cerebrospinal fluid (in mM: 125 NaCl, 2.5 KCl, 2 $CaCl_2$, 1.3 $MgCl_2$, 1.3 NaH_2PO_4, 1.3 Na-ascorbate, 0.6 Na-pyruvate, 25 glucose and 25 $NaHCO_3$) for at least 1 h before recording. Slices were transferred to a recording chamber and superfused with 2 ml min^{-1} artificial cerebrospinal fluid. Patch pipettes (3-6 MΩ) were made of borosilicate glass (BF150-86-10, Sutter Instruments). For recording of action potential firing, the

pipettes were filled with a K-based internal solution containing (in mM) 130 K-gluconate, 10 KCl, 10 HEPES, 1 EGTA, 2 Mg-ATP, 0.3 Na-GTP, 2 $MgCl_2$, 290 mOsm kg^{-1}, adjusted to pH 7.3 with KOH. For the postsynaptic current recording, pipettes were filled with a Cs-based low Cl^- internal solution containing (in mM) 135 $CsMeSO_3$, 10 HEPES, 1 EGTA, 3.3 QX-314, 4 Mg-ATP, 0.3 Na-GTP, 8 Na_2-phosphocreatine, 290 mOsm kg^{-1}, adjusted to pH 7.3 with CsOH. In some experiments, the APV, CNQX, TTX or picrotoxin blockers were applied by bath perfusion. Whole-cell voltage-clamp recordings were performed at room temperature (22–25 °C) using a Multiclamp 700B amplifier and a Digidata 1550B (Molecular Devices). Data were sampled at 10 kHz and analyzed using pClamp10 (Molecular Devices). For the optogenetic experiments, a blue light-emitting diode (470 nm, Thorlabs) controlled by digital commands from the Digidata 1550B was coupled to the microscope via a dual lamp house adaptor (5-UL180, Olympus) to deliver photostimulation. To record light-evoked EPSCs and IPSCs, 2 ms, 0.5-2 mW blue light was delivered through the objective to illuminate the entire field of view. The membrane potential was held at -70 mV to record EPSCs and at 0 mV to record $GABA_A$ receptor-mediated IPSCs. Individual sweeps were separated by 15 s. Event analysis was performed using pClamp10 and Axograph 1.7.6 software, with a matching threshold of 2.8 was applied to minimize false-positives.

Morphology

The intracellular solution containing 0.1% Lucifer yellow (Sigma, L0144) was used to inject dye into PVT neurons for whole-cell recording. After recording, the brain slices were fixed in 4% paraformaldehyde overnight. To enhance the intensity and persistence of the fluorescence, anti-lucifer yellow antibody (Invitrogen, A5750, rabbit, 1:500) was used for further staining, and the secondary antibody was conjugated with Alexa Fluor 488 (Invitrogen, A-11008, 1:500). The labelled cells were imaged using a fluorescence microscope (Olympus, BX53).

Single-cell real-time PCR

At the end of each recording, the cytoplasm was aspirated into the patch pipette and ejected into a PCR tube. The single-cell real-time PCR protocol was designed to detect the presence of mRNAs encoding for opioid receptors. Preamplification and real-time PCR were performed with gene-specific TaqMan® assays (Thermo Fisher, 4453320 Mm01188089_m1) using the Single Cell-to-CT^{TM} kit (Invitrogen, 4458237) according to the manufacturer's protocol. Amplification products were visualized by electrophoresis on a 2% agarose gel. Care was taken to minimize RNA degradation and contamination during the single-cell real-time PCR procedures.

Stereotaxic surgery

Adult mice were anesthetized with 2% isoflurane and placed in a stereotactic instrument (RWD, Shenzhen, China). Microinjections were performed using a 33-gauge needle connected to a 10 μl Hamilton syringe. Virus was injected into the PVT (bregma -1.0 mm; lateral 0.3 mm; ventral 3.0 mm, with a 5° angle from the

center to the sides) and zona incerta (bregma -1.0 mm; lateral 0.7 mm; ventral -4.4 mm). The target site was injected with 200 nl of purified and concentrated AAV (10^{12} IU/ml) with a slow injection rate (100 nl/min). The injection capillary was removed 5 min after the end of the injection. All mice were allowed to recover at least 3 weeks before electrophysiological recording. Histological slides were examined blindly for EGFP or mCherry expression. Only the mice with virus infection at the correct site were selected for further analysis.

Immunostaining

Mice were anesthetized with pentobarbital sodium (0.8%) and perfused with 4% paraformaldehyde. Brains were post-fixed overnight. Coronal sections of 50 μm thickness were cut on a freezing microtome. Sections were incubated with primary antibodies for 24 hours at 4 °C. The primary antibodies were c-Fos (Cell Signaling, 2250s, rabbit, 1:1000), NeuN (Millipore, MAB377, mouse, 1:500), and μ-opioid receptor (MOR) antibody (ImmunoStar, 24216, rabbit, 1:1000). Secondary antibodies were conjugated to Alexa Fluor (Invitrogen, 1:500). Sections were mounted in Fluoroshield (Sigma). Images were captured using a 63x objective on a Zeiss LSM880 confocal microscope. Data were analyzed using ImageJ.

Statistical analysis

Data are presented throughout as the mean ± SEM. Unless otherwise noted, male and female mice were used in all studies. No sex differences were observed for any of the parameters measured and therefore data from male and female mice were pooled

to increase statistical power. Electrophysiological data were analyzed using Student's t test and ANOVA test. For all statistical comparisons, differences were considered as significant at $P < 0.05$. df: degrees of freedom.

Results

Opioid receptors modulate the activity of PVT neurons

To investigate the effects of opioid on the activity of PVT neurons, mice were injected intraperitoneally (i.p.) with morphine (10 mg/kg) to induce expression of the immediate early gene c-Fos in the brain, which is a marker of recent neuronal activity (Zhu et al., 2016). After 90 minutes, mice were anesthetized and perfused with 4% formaldehyde, and then frozen brains were sectioned and immunostained with antibodies. Morphine injection increased the proportion of cells expressing c-Fos in the PVT compared to saline injection (saline, 101.8 ± 11.57 % vs. morphine, 167.5 ± 13.75 %, $P = 0.0016$, $t = 3.676$, $df = 19$, $n = 2$ mice each group, unpaired t test) (Fig. 1A,B), indicating that morphine activates PVT neurons. Morphine acts through opioid receptors that couple to G protein-gated inwardly rectifying potassium (GIRK) channels, inhibiting neuronal activity (Cruz et al., 2008; Kotecki et al., 2015; Rifkin et al., 2017). High expression of opioid receptors has been reported in PVT (George et al., 1994; Mansour et al., 1994). To investigate the functions of opioid receptors in PVT, we performed whole-cell patch clamp recordings in brain slices. First, we recorded the action potential firing of PVT neurons. The firing rate was significantly reduced in

most PVT cells after application of morphine (30 μM) (ACSF, 5.06 ± 0.42 Hz, n = 16 vs. morphine, 1.64 ± 0.60 Hz, n = 16 vs. morphine + naloxone, 4.27 ± 0.55 Hz, n = 8. One-way ANOVA, $F_{(1, 16)} = 19.63$, P = 0.0002, followed by post-hoc Tukey's test) (Fig. 1C,E), which can be reversed by application of the opioid receptor antagonist naloxone (10 μM). The subtype of opioid receptors involved in the regulation of PVT neuronal activity was then determined. Three subtype agonists were used to record firings of PVT neurons, including the MOR agonist DAMGO ([D-Ala^2, N-Me-Phe^4, Gly^5-ol]-enkephalin, 1 μM), the KOR agonist U50488 (1 μM), and the DOR agonist SNC80 (3 μM). DAMGO application significantly reduced the firing rate in most PVT cells, similar to the effect of morphine (ACSF, 5.17 ± 0.39 Hz, n = 16 vs. DAMGO, 2.33 ± 0.77 Hz, n = 16 vs. DAMGO + naloxone, 3.82 ± 0.30 Hz, n = 12. One-way ANOVA, $F_{(1, 19)} = 22.04$, P < 0.0001, followed by post-hoc Tukey's test) (Fig. 1D,F). However, the KOR agonist U50488 and the DOR agonist SNC80 had no effect on the firing rate of PVT neurons (ACSF, 5.92 ± 0.54 Hz vs. U50488, 6.31 ± 0.59 Hz, n = 10, P = 0.4278, t = 0.83, df = 9; ACSF, 6.13 ± 0.61 Hz vs. SNC80, 5.63 ± 0.60 Hz, n = 10, P = 0.1679, t = 1.5, df = 9, paired t test) (Fig. 1G,H). These results suggest that the MOR is important in regulating the activities of PVT neurons.

Interestingly, a few cells had no apparent response to morphine or DAMGO. To investigate the difference between these opioid sensitive and insensitive neurons, we first examined the morphology of PVT neurons. Lucifer yellow CH dipotassium salt was added to the intracellular pipette solution during recording, and then brain slices

were then immunostained with Lucifer yellow antibody to enhance the fluorescence. However, we did not see a clear difference in the morphology between these two groups of PVT neurons (examples are shown in Fig. 1I). Second, not all PVT neurons may express MORs. To investigate the difference in MOR expression in these two groups, we performed single-cell real-time (RT) PCR after recording. The single-cell RT PCR procedure is shown in Fig. 1J. Both the cells that were sensitive to DAMGO and also the cells that showed no response to DAMGO expressed *Oprm1* (the gene encoding MOR), suggesting that MORs were widely expressed in the PVT neurons. Since the RT-PCR revealed the expression of MORs in the PVT neurons, hence the postsynaptic modulation, the insensitive neurons might reflect that the MORs were not functional or there might be some presynaptic mechanism to counteract it. Previous literature has reported that MORs could also be expressed presynaptically to regulate firing, and that opioid receptors may be involved in regulating synaptic inputs to the PVT.

Opioid receptors modulate inhibitory synaptic inputs to the PVT

Opioid receptors have been reported to modulate synaptic transmission, particularly GABAergic inhibitory transmission (Fields and Margolis, 2015; Jiang et al., 2021). To assess the effects of opioid receptors on synaptic transmission in the PVT, we first recorded spontaneous excitatory and inhibitory postsynaptic currents (sEPSCs and sIPSCs). Bath application of morphine (30 μM) did not alter the frequency or

amplitude of sEPSCs (Amplitude: ACSF, 11.09 ± 0.72 pA vs. morphine, 10.45 ± 0.56 pA, n = 14, P = 0.444, t = 0.79, df = 13; Frequency: ACSF, 4.94 ± 0.59 Hz vs. morphine, 4.53 ± 0.53 Hz, n = 14, P = 0.1824, t = 1.41, df = 13, paired t test) (Fig. 2A-C), but decreased the frequency and amplitude of sIPSCs (Amplitude: ACSF, 13.30 ± 0.91 pA vs. morphine, 11.89 ± 0.66 pA, n = 18, P = 0.0078, t = 3.01, df = 17; Frequency: ACSF, 4.03 ± 0.90 Hz vs. morphine, 3.31 ± 0.68 Hz, n = 18, P = 0.0133, t = 2.76, df = 17, paired t test) (Fig. 2D-F). Thus, opioid receptors can regulate inhibitory synaptic transmission in the PVT. To further investigate which subtype of opioid receptors contributes to the regulation of inhibitory inputs to the PVT, we recorded miniature IPSCs (mIPSCs) in the presence of APV (NMDA receptor antagonist, 50 μM), CNQX (AMPA receptor antagonist, 10 μM) and TTX (sodium channel blocker, 0.5 μM). Morphine (30 μM) also decreased the frequency and amplitude of mIPSCs in the PVT neurons (Amplitude: ACSF, 8.32 ± 0.54 pA vs. morphine, 7.52 ± 0.54 pA, n = 10, P = 0.0015, t = 4.48, df = 9; Frequency: ACSF, 2.88 ± 0.31 Hz vs. morphine, 2.34 ± 0.33 Hz, n = 10, P = 0.0028, t = 4.07, df = 9, paired t test) (Fig. 3A,B). The MOR agonist DAMGO (1 μM) significantly reduced both the amplitude and frequency of mIPSCs in the PVT (Amplitude: ACSF, 9.57 ± 0.85 pA vs. DAMGO, 8.71 ± 0.75 pA, n = 12, P = 0.0353, t = 2.4, df = 11; Frequency: ACSF, 2.66 ± 0.38 Hz vs. DAMGO, 2.04 ± 0.41 Hz, n = 12, P = 0.0006, t = 4.73, df = 11, paired t test) (Fig. 3C,D). The KOR agonist U50488 (1 μM) also significantly reduced the amplitude and frequency of mIPSCs in the PVT (Amplitude: ACSF, 11.48

± 0.75 pA vs. U50488, 10.02 ± 0.64 pA, n = 12, P = 0.0005, t = 4.9, df = 11; Frequency: ACSF, 4.35 ± 0.97 Hz vs. U50488, 3.11 ± 0.70 Hz, n = 12, P = 0.0014, t = 4.26, df = 11, paired t test) (Fig. 3E,F). There was no effect of the DOR agonist SNC80 (3 μM) on the mIPSCs (Amplitude: ACSF, 13.94 ± 1.07 pA vs. SNC80, 13.42 ± 1.01 pA, n = 12, P = 0.0965, t = 1.82, df = 11; Frequency: ACSF, 4.95 ± 0.64 Hz vs. SNC80, 4.75 ± 0.51 Hz, n = 12, P = 0.4612, t = 0.76, df = 11, paired t test) (Fig. 3G,H). These results suggest that MOR and KOR are involved in the modulation of inhibitory synaptic inputs to the PVT.

KOR modulates inhibitory synaptic transmission from the ZI to the PVT

To explore the source of the inhibitory inputs to the PVT, we performed retrograde tracing in transgenic mice. Cre-dependent retro-AAV-DIO-EGFP was injected into the PVT of GAD2-Cre mice (Fig. 4A). With this tracing strategy, only GABAergic neurons that project to the PVT are labelled with GFP. After 2-3 weeks of infection, we sectioned the whole brains of these mice and examined the distribution of GFP fluorescence. A few brain areas were found to have intense GFP-expressing neurons (Fig. 4B), including the suprachiasmatic nucleus (SCN), the zona incerta (ZI) and the dorsal raphe (DR). The ZI is an inhibitory subthalamic region with extensive connections throughout the brain. Recent studies have demonstrated diverse functions of the ZI in processing sensory information, regulating behavior, mediating motivational states, and participating in neural plasticity (Wang et al., 2020).

316 Projections from ZI to PVT can reliably produce rapid and substantial eating (Zhang
317 and van den Pol, 2017). MOR and KOR are expressed in the ZI of rats and mice
318 (DePaoli et al., 1994; George et al., 1994; Mansour et al., 1994; Jenab et al., 1995),
319 but little is known about the function of opioid receptors in the ZI-to-PVT pathway.

320 To test whether opioid receptors regulate GABAergic inputs from the ZI to the
321 PVT, ZI neurons were transduced with AAV-DIO-ChR2-mCherry (Fig. 4C), and
322 optogenetic experiments were performed in the PVT brain slice 3-4 weeks after
323 surgery. A brief pulse of blue light (470 nm, 2 ms) evoked robust inhibitory
324 postsynaptic currents (oIPSCs) in PVT neurons when clamped at 0 mV (Fig. 4D,
325 upper panel), which can be blocked by the $GABA_A$ receptor antagonist picrotoxin
326 (100 μM) (Fig. 4D, lower panel). Light stimulation did not evoke any detectable
327 EPSCs when clamped at -70 mV (Fig. 4D, upper panel). The oIPSCs were preserved
328 in the presence of TTX (1 μM) and 4-AP (1 mM), suggesting that the ZI to PVT input
329 is monosynaptic (ACSF, 339.0 ± 74.10 pA vs. TTX and 4-AP, 344.2 ± 54.05 pA, n
330 = 8, P = 0.8725, t = 0.17, df = 7, paired t test) (Fig. 4E,F). We found that DAMGO (1
331 μM) had no effect on the amplitude and paired-pulse ratio (PPR) of oIPSCs from ZI
332 to PVT (Amplitude: ACSF, 164.7 ± 34.95 pA vs. DAMGO, 185.0 ± 42.65 pA, n = 13,
333 P = 0.2109, t = 1.32, df = 12; PPR: ACSF, 1.02 ± 0.08 vs. DAMGO, 1.01 ± 0.071, n =
334 13, P = 0.861, t = 0.18, df = 12, paired t test) (Fig. 4H,I). The KOR agonist U50488 (1
335 μM) significantly reduced the amplitude of oIPSCs but did not alter the PPR
336 (Amplitude: ACSF, 134.0 ± 21.08 pA vs. U50488, 105.3 ± 20.16 pA, n = 11, P =

0.0123, t = 3.05, df = 10; PPR: ACSF, 1.02 ± 0.05 vs. U50488, 1.12 ± 0.12, n = 11, P = 0.3107, t = 1.07, df = 10, paired t test) (Fig. 4J,K). Thus, KOR activation suppressed the GABAergic inputs to the PVT, suggesting that KOR can modulate the inhibitory transmission in the ZI to PVT pathway. Surprisingly, the PPR at ZI synapses to PVT neurons was not altered. As opioid receptors are both presynaptic- and postsynaptic-located in the PVT, it is possible that MOR or KOR agonists act on both the presynaptic and postsynaptic receptors and counteract the change in PPR.

Chronic morphine exposure reduced the inhibition of firing by MOR

Opioids are currently the most effective drugs for pain relief. However, they are also rewarding, and their repeated use can lead to dependence and addiction (Fields and Margolis, 2015). Addiction is a complex, relapsing disorder in which drugs of abuse hijack, overstimulate and compromise reward-processing systems and associated networks (Darcq and Kieffer, 2018). Activation of the PVT can induce aversion and contribute to opioid withdrawal (Zhu et al., 2016). In our results, acute morphine could modulate the activities of PVT neurons. To investigate the functions of opioid receptors after chronic morphine treatment, mice were rendered opiate dependent by daily i.p. injections of morphine in their home cage with doses escalating from 10 to 50 mg per kg body weight (Zhu et al., 2016) (Fig. 5A). Control mice were i.p. injected with the same volume of saline. On day 7, whole-cell recording was performed in brain slices, and the activities of PVT neurons before and

after MOR agonist application were tested. Representative recordings are shown in the Fig. 5D and 5E. DAMGO application significantly reduced the firing rate of PVT neurons in the saline-treated mice (ACSF, 2.91 ± 0.33 Hz vs. DAMGO, 0.64 ± 0.34 Hz vs. DAMGO + Naloxone, 2.53 ± 0.37 Hz; n = 12. One-way ANOVA, $F_{(1, 14)}$ = 22.93, P = 0.0001, followed by post-hoc Tukey's test) (Fig. 5B), and this effect was largely suppressed in the morphine-treated mice (ACSF, 4.79 ± 0.36 Hz vs. DAMGO, 3.66 ± 0.61 Hz vs. DAMGO + Naloxone, 4.73 ± 0.34 Hz; n = 15. One-way ANOVA, $F_{(1, 18)}$ = 5.998, P = 0.0184, followed by post-hoc Tukey's test) (Fig. 5C).

As the recordings were made 2 days after the last morphine injection (Fig. 5A), the animal could be in a state of spontaneous withdrawal. To discriminate between desensitization effects due to morphine exposure and spontaneous withdrawal, we performed recordings from chronic morphine exposure mice in which the brain slices were prepared two hours after the last morphine injection on day 5 (Fig. 5F). DAMGO did not reduce the firing rates in the morphine exposure group (ACSF, 3.03 ± 0.25 Hz vs. DAMGO, 2.25 ± 0.44 Hz vs. DAMGO + Naloxone, 2.91 ±0.22 Hz; n = 9. One-way ANOVA, $F_{(1, 12)}$ = 2.339, P = 0.1472, followed by post-hoc Tukey's test) (Fig. 5H). In addition, we examined the effects of DAMGO on firing when animals were in a state of naloxone-precipitated withdrawal. Mice were i.p. injected with naloxone (5 mg/kg) two hours after the last morphine injection, and 10 - 15 min later, the animals were anesthetized and decapitated for preparation of brain slices (Zhu et al., 2016) (Fig. 5G). DAMGO also did not reduce the firing rates in these

naloxone-precipitated withdrawal mice (ACSF, 3.59 ± 0.33 Hz vs. DAMGO, 2.71 ± 0.56 Hz vs. DAMGO + Naloxone, 3.73 ±0.30 Hz; n = 6. One-way ANOVA, $F_{(1, 6)}$ = 6.134, P = 0.0466, followed by post-hoc Tukey's test) (Fig. 5I). Furthermore, the degree of suppression, as quantified by suppression ratios (ratios between the firing rate in ACSF and DAMGO conditions), was similar in the morphine treatment, morphine exposure and naloxone-precipitated withdrawal groups, and all changed less than in the saline treatment group (saline treatment, 0.18 ± 0.09, n = 12 vs. morphine treatment, 0.74 ± 0.10, n = 15 vs. morphine exposure, 0.75 ± 0.12, n = 9 vs. naloxone-precipitated withdrawal, 0.74 ± 0.13, n = 6. One-way ANOVA, $F_{(2, 14)}$ = 7.797, P = 0.0063, followed by post-hoc Dunnett's test) (Fig. 5J). As the reduction in DAMGO inhibition was already present on day 5 in the morphine exposure group, without any withdrawal effect, the reduction in firing rate on day 7 in the morphine treatment group was more likely due to morphine exposure rather than spontaneous opioid withdrawal.

Opioid receptors are members of the G protein-coupled receptor (GPCR) family, and they can activate G protein-activated inwardly rectifying potassium (GIRK) channels via G proteins. Activation of GIRK channels induces membrane hyperpolarization of the neurons via K^+ efflux and reduces neuronal excitability (Ikeda et al., 2002; Rifkin et al., 2017). Since opioids act through MORs that couple to GIRK channels, we asked whether the reduced inhibition of firing rate by DAMGO is due to the reduced MOR coupling to GIRK after chronic morphine treatment? We

recorded GIRK currents induced by DAMGO (3 μM) when the membrane potential was clamped at -60 mV. DAMGO application induced robust outward GIRK currents in saline-treated control mice (Fig. 5K, black). DAMGO application also induced significant GIRK currents in morphine-treated and morphine-exposed mice, and the amplitudes were similar to those in saline-treated mice (Fig. 5K,L). However, DAMGO could not induce obvious GIRK currents in the naloxone-precipitated withdrawal mice (saline treatment, 19.09 ± 4.03 pA, n = 9 vs. morphine treatment, 22.67 ± 3.29 pA, n = 11 vs. morphine exposure, 15.32 ± 4.45 pA, n = 7 vs. naloxone-precipitated withdrawal, 2.82 ± 1.96 pA, n = 6. One-way ANOVA, $F_{(2, 16)}$ = 4.714, P = 0.0288, followed by post-hoc Dunnett's test) (Fig. 5K,L). Thus, the results showed that DAMGO-induced GIRK currents were reduced in naloxone-precipitated withdrawal mice, suggesting a decoupling of MOR and GIRK induced by naloxone-precipitated withdrawal.

To confirm the contribution of GIRK channels to the DAMGO inhibition, we used a GIRK channel antagonist, tertiapin-Q, to reverse DAMGO-induced inhibition of PVT neurons. As we have shown previously, DAMGO suppressed the firing and hyperpolarized PVT neurons (Fig. 5M). Application of tertiapin-Q (1 μM) did not restore the action potential firing (ACSF, 3.28 ± 0.33 Hz vs. DAMGO, 0.18 ± 0.18 Hz vs. DAMGO + Tertiapin-Q, 0.60 ± 0.56 Hz, n = 5. One-way ANOVA, $F_{(1, 5)}$ = 27.05, P = 0.0028, followed by post-hoc Tukey's test) (Fig. 5N), but partially reversed the hyperpolarization of the membrane potential (ACSF, -40.29 ± 1.93 mV vs. DAMGO,

-49.27 ± 2.22 mV vs. DAMGO + Tertiapin-Q, -43.39 ± 1.11 mV, n = 5. One-way ANOVA, $F_{(1, 6)}$ = 11.82, P = 0.0118, followed by post-hoc Tukey's test) (Fig. 5O). These results suggest that GIRK channels contribute to membrane potential hyperpolarization, but not to the firing suppression effect of DAMGO on PVT neurons. We didn't see any GIRK currents induced by the KOR agonist U50488 (3 μM) (Fig. 5K, green).

Prolonged use of opioids leads to a reduction in their effectiveness, known as tolerance, and research has been devoted to elucidating the molecular basis of desensitization (Marie et al., 2006). The MOR mediates both presynaptic inhibition and postsynaptic neuromodulatory effects of endogenous opioid peptides (Kieffer and Evans, 2009; Corder et al., 2018; Darcq and Kieffer, 2018). The mechanism underlying postsynaptic MOR desensitization is based on ligand-induced phosphorylation of the MOR cytoplasmic tail by GPCR kinases (GRKs) followed by receptor internalization (Gainetdinov et al., 2004; Just et al., 2013; Williams et al., 2013; Yousuf et al., 2015; Arttamangkul et al., 2018; Jullie et al., 2020). To investigate whether MOR is internalized in PVT neurons after chronic morphine exposure, MOR antibody was used to show the distribution of MOR, and NeuN antibody was used to show the soma of the neurons (Fig. 6A). Radius analysis shows the distribution of MOR from the center to the periphery of the PVT cells (n = 8 cells per group). In the chronic morphine treatment group, MORs were scattered in the cell body (cytoplasm), whereas in the saline treatment group, MORs were mostly

distributed across the periphery (membrane) (Cytoplasm area: morphine treatment, 47.67 ± 1.78 vs. saline treatment, 36.39 ± 1.18, n = 8; Membrane area: morphine treatment, 45.94 ± 0.43 vs. saline treatment, 67.80 ± 0.73, n = 8. Two-way ANOVA followed by post-hoc Tukey's test; drug treatment × cellular location, $F_{(1, 8)} = 181.7$, $P < 0.0001$; drug treatment, $F_{(1, 8)} = 24.9$, $P < 0.01$; cellular location, $F_{(1, 8)} = 145.8$, $P < 0.0001$) (Fig. 6B,C). Thus, chronic morphine treatment induced the internalization of MORs in the PVT neurons and reduced the postsynaptic neuromodulatory effects of opioids.

Chronic morphine exposure reduced the modulation of inhibitory inputs by MOR and KOR

Previously, we found that opioid receptors contribute to the modulation of inhibitory inputs to the PVT in wild-type mice. Could opioid receptors still modulate the inhibitory transmission in the PVT after chronic morphine treatment? DAMGO (1 μM) reduced the amplitude and frequency of mIPSCs in saline-treated mice (Amplitude: ACSF, 9.01 ± 0.82 pA vs. DAMGO, 8.55 ± 0.82 pA, n = 11, P = 0.0459, t = 2.28, df = 10; Frequency: ACSF, 3.76 ± 0.85 Hz vs. DAMGO, 3.52 ± 0.83 Hz, n = 11, P = 0.006, t = 3.47, df = 10, paired t test) (Fig. 7A,C,D), consistent with what we found in wild type mice. U50488 (1 μM) also decreased the amplitude and frequency of mIPSCs in saline-treated mice (Amplitude: ACSF, 8.30 ± 0.44 pA vs. U50488, 7.44 ± 0.40 pA, n = 13, P = 0.0013, t = 4.19, df = 12; Frequency: ACSF, 4.01 ± 0.56

Hz vs. U50488, 3.01 ± 0.44 Hz, n = 13, P = 0.0077, t = 3.19, df = 12, paired t test) (Fig. 7B,E,F). Different from the control saline treatment group, the suppressive effects of DAMGO on mIPSCs were diminished after chronic morphine treatment (Amplitude: ACSF, 9.66 ± 0.79 pA vs. DAMGO, 9.11 ± 0.66 pA, n = 12, P = 0.0794, t = 1.93, df = 11; Frequency: ACSF, 4.33 ± 0.78 Hz vs. DAMGO, 3.81 ± 0.72 Hz, n = 12, P = 0.0544, t = 2.15, df = 11, paired t test) (Fig. 7G,I,J). The effects of U50488 (1 μM) were also attenuated after chronic morphine treatment (Amplitude: ACSF, 8.31 ± 0.86 pA vs. U50488, 8.05 ± 0.80 pA, n = 12, P = 0.266, t = 1.17, df = 11; Frequency: ACSF, 2.94 ± 0.56 Hz vs. U50488, 2.63 ± 0.54 Hz, n = 12, P = 0.0495, t = 2.21, df = 11, paired t test) (Fig. 7H,K,L). The modulation of inhibitory inputs by MOR and KOR were reduced in morphine-treated mice, suggesting that the involvement of MOR and KOR in PVT was reduced after chronic morphine exposure.

Is the kappa opioid regulation of the ZI to PVT input sensitive to chronic morphine exposure? Optically evoked IPSCs were recorded from saline or morphine treated mice. U50488 (1 μM) reduced the amplitude of oIPSCs from ZI to PVT in the saline treatment mice (ACSF, 255.3 ± 21.94 pA vs. U50488, 205.9 ± 19.36 pA, n = 20, P = 0.00007, t = 5.06, df = 19, paired t test) (Fig. 7M, left), but this effect was reduced by chronic morphine treatment (ACSF, 108.2 ± 13.85 pA vs. U50488, 103.2 ± 14.03 pA, n = 19, P = 0.2403, t = 1.21, df = 18, paired t test) (Fig. 7N, left). As in wild-type mice, U50488 did not alter the paired-pulse ratio (PPR) in both saline-treated and morphine-treated mice (Saline treatment: ACSF, 0.91 ± 0.04 vs.

U50488, 0.91 ± 0.03, n = 20, P = 0.7451, t = 0.33, df = 19; Morphine treatment: ACSF, 1.08 ± 0.12 vs. U50488, 1.19 ± 0.13 , n = 14, P = 0.196, t = 1.36, df = 13, paired t test) (Fig. 7M,N). These results suggest that KOR is important in modulating inhibitory input from the ZI to the PVT and that chronic morphine exposure can disinhibit the ZI to PVT pathway.

Discussion

The PVT serves as a key node in the neural circuits that regulate addictive behaviors. In addition to the acute effects of drugs, PVT neurons are also recruited at different stages of the drug addiction cycle (Zhou and Zhu, 2019). In this study, we investigated the effects of morphine and opioid receptor agonists on the activities of PVT neurons. Bath-applied morphine and the MOR agonist DAMGO reduced the activities of PVT neurons in brain slices. Furthermore, MOR and KOR were also involved in modulating inhibitory inputs to the PVT. Prolonged morphine use decreased the contribution of opioid receptors in the PVT. We did not observe any involvement of DOR in the regulation of PVT activities. Our results showed that MOR and KOR are essential in the regulation of PVT activities.

Neurons in the PVT are primarily glutamatergic and receive GABAergic inputs from other nuclei, such as the ZI. We found that KOR can regulate the inhibitory projection from the ZI to the PVT. The ZI is also an integrative node for behavioral modulation and an inhibitory subthalamic region connecting with many brain areas

(Wang et al., 2020). Recently, different action sequences based on the motivational level of novelty seeking have been revealed, and a circuit underlying curiosity and novelty-seeking behavior requires a subpopulation of medial ZI neurons (Ahmadlou et al., 2021). PVT neurons encode multiple salient features of sensory stimuli, including reward, aversion and novelty, and weigh the valence between the positive and negative information (Zhu et al., 2018). We found that activation of opioid receptors in the terminals of ZI neurons reduced the inhibitory inputs to the PVT, which could disinhibit the activities of PVT neurons. Thus, the ZI to the PVT pathway may be important for motivational behavior, and the opioid system in this pathway may influence behavioral responses to dynamic environmental contexts.

Opioid receptors are members of the G protein-coupled receptor (GPCR) family, and they can activate G protein-activated inwardly rectifying potassium (GIRK) channels via G proteins. Activation of GIRK channels induces membrane hyperpolarization of the neurons via K^+ efflux and reduces neuronal excitability (Ikeda et al., 2002; Rifkin et al., 2017). We applied the MOR agonist DAMGO and the GIRK channel antagonist tertiapin-Q to brain slices. DAMGO application decreased the firing rate and hyperpolarized the membrane potential of PVT neurons. Tertiapin-Q reversed the hyperpolarization induced by DAMGO, but failed to restore the firing in most of the cells. We therefore proposed that activation of GIRK channels is the underlying mechanism for membrane potential hyperpolarization, but other mechanisms such as a decrease in calcium conductance may contribute to the reduction

in firing rate upon MOR activation (Borgland, 2001), which require future investigation.

Chronic morphine exposure induces adaptive phenomena such as tolerance and dependence. In tolerance, more morphine is required to achieve the initial effect, whereas dependence is manifested by the withdrawal syndrome induced by cessation of morphine exposure (Cruz et al., 2008). To distinguish between the effects of morphine tolerance and withdrawal, we compared the results between the morphine exposure group and the naloxone-precipitated withdrawal group. As in the morphine treatment group (2 days after the last morphine injection), the decrease in firing rate induced by DAMGO was dramatically attenuated in both the morphine exposure and naloxone-precipitated withdrawal groups. Thus, these results suggest that, the reduced inhibition of firing rate by DAMGO is due to chronic morphine exposure rather than spontaneous withdrawal.

We also found that DAMGO was able to induce robust GIRK currents with similar amplitudes in the saline-treated, morphine-treated and morphine-exposed mice. MOR coupling to GIRKs was not desensitized by chronic treatment, suggesting that other intracellular downstream effectors such as adenylyl cyclase, voltage-gated Ca^{2+} channels and others (Williams et al., 2001) play more important roles in MOR desensitization. However, DAMGO failed to evoke any apparent outward currents in the naloxone-precipitated withdrawal mice, suggesting that the coupling of MOR to GIRK channels was reduced in these mice. This result indicates that naloxone induces

uncoupling of MORs and GIRKs. Naloxone might suppress functional GIRK channels, probably through a compensatory mechanism involving internalization and phosphorylation of GIRK channels (Hearing et al., 2013). These results were also consistent with previous report highlighting the importance of GIRK in the naloxone-precipitated morphine withdrawal (Cruz et al., 2008).

Desensitization of opioid receptors is thought to be required for tolerance and involves phosphorylation by kinases and uncoupling from G-proteins realized by arrestins (Marie et al., 2006). Internalization or endocytosis of GPCRs is another common way to regulate their activity by removing active receptors from the cell surface into the intracellular space. GPCR internalization is mediated by clathrin-coated pits, caveolae and uncoated vesicles (Claing et al., 2002). Opioid receptors rapidly diffuse across the axon surface and internalize specifically at presynaptic terminals following ligand-induced activation (Jullie et al., 2020). In this study, the effects of opioid receptor agonists on the excitability and inhibitory inputs of PVT neurons were attenuated after chronic morphine exposure. These results may be due to desensitization and internalization of opioid receptors. The diminished effects of firing could also be caused by possible changes in opioid regulation of presynaptic inputs, as our recordings were made in the absence of synaptic blockers.

A previous study demonstrated a morphine-induced increase in the firing rate of PVT neurons, which was only observed during the light cycle, but not the dark cycle (McDevitt and Graziane, 2019). This study compared the firing rate between the

saline-treated and morphine-treated mice, which reflects contributions from several factors including synaptic inputs, intrinsic excitability, opioid and other neuromodulation. We did the recording during the light cycle, but the differences were that we applied opioid agonists and antagonists in the brain slices, directly probe the function of opioid receptors in the PVT. Our study also revealed the changes in opioid modulation of PVT activities induced by chronic morphine treatment.

Together, MOR and KOR contribute to the modulation of PVT activities and inhibitory synaptic inputs, and these effects can be reduced by chronic morphine exposure.

References

Ahmadlou M, Houba JHW, van Vierbergen JFM, Giannouli M, Gimenez GA, van Weeghel C, Darbanfouladi M, Shirazi MY, Dziubek J, Kacem M, de Winter F, Heimel JA (2021) A cell type-specific cortico-subcortical brain circuit for investigatory and novelty-seeking behavior. Science 372.

Arttamangkul S, Heinz DA, Bunzow JR, Song X, Williams JT (2018) Cellular tolerance at the micro-opioid receptor is phosphorylation dependent. Elife 7.

Baimel C, Borgland SL (2015) Orexin Signaling in the VTA Gates Morphine-Induced Synaptic Plasticity. J Neurosci 35:7295-7303.

Barson JR, Mack NR, Gao WJ (2020) The Paraventricular Nucleus of the Thalamus Is an Important Node in the Emotional Processing Network. Front Behav Neurosci 14:598469.

Bengoetxea X, Goedecke L, Blaesse P, Pape HC, Jungling K (2020) The micro-opioid system in midline thalamic nuclei modulates defence strategies towards a conditioned fear stimulus in male mice. J Psychopharmacol 34:1280-1288.

Borgland SL (2001) Acute opioid receptor desensitization and tolerance: is there a link? Clin Exp Pharmacol Physiol 28:147-154.

Brunton J, Charpak S (1998) mu-Opioid peptides inhibit thalamic neurons. J Neurosci 18:1671-1678.

Chen Z, Tang Y, Tao H, Li C, Zhang X, Liu Y (2015) Dynorphin activation of kappa opioid receptor reduces neuronal excitability in the paraventricular nucleus of mouse thalamus. Neuropharmacology 97:259-269.

Choi EA, Jean-Richard-Dit-Bressel P, Clifford CWG, McNally GP (2019) Paraventricular Thalamus Controls Behavior during Motivational Conflict. J Neurosci 39:4945-4958.

Claing A, Laporte SA, Caron MG, Lefkowitz RJ (2002) Endocytosis of G protein-coupled receptors: roles of G protein-coupled receptor kinases and beta-arrestin proteins. Prog Neurobiol 66:61-79.

Corder G, Castro DC, Bruchas MR, Scherrer G (2018) Endogenous and Exogenous Opioids in Pain. Annu Rev Neurosci 41:453-473.

Cruz HG, Berton F, Sollini M, Blanchet C, Pravetoni M, Wickman K, Luscher C (2008) Absence and rescue of morphine withdrawal in GIRK/Kir3 knock-out mice. J Neurosci 28:4069-4077.

Darcq E, Kieffer BL (2018) Opioid receptors: drivers to addiction? Nat Rev Neurosci 19:499-514.

DePaoli AM, Hurley KM, Yasada K, Reisine T, Bell G (1994) Distribution of kappa opioid receptor mRNA in adult mouse brain: an in situ hybridization histochemistry study. Mol Cell Neurosci 5:327-335.

Deutch AY, Bubser M, Young CD (1998) Psychostimulant-induced Fos protein expression in the thalamic paraventricular nucleus. J Neurosci 18:10680-10687.

618 Do-Monte FH, Minier-Toribio A, Quinones-Laracuente K, Medina-Colon EM, Quirk
619 GJ (2017) Thalamic Regulation of Sucrose Seeking during Unexpected Reward
620 Omission. Neuron 94:388-400 e384.
621 Fields HL, Margolis EB (2015) Understanding opioid reward. Trends Neurosci
622 38:217-225.
623 Flagel SB (2022) The paraventricular nucleus of the thalamus and its potential role in
624 psychopathology. Neuropsychopharmacology 47:385-386.
625 Gainetdinov RR, Premont RT, Bohn LM, Lefkowitz RJ, Caron MG (2004)
626 Desensitization of G protein-coupled receptors and neuronal functions. Annu
627 Rev Neurosci 27:107-144.
628 George SR, Zastawny RL, Briones-Urbina R, Cheng R, Nguyen T, Heiber M, Kouvelas
629 A, Chan AS, O'Dowd BF (1994) Distinct distributions of mu, delta and kappa
630 opioid receptor mRNA in rat brain. Biochem Biophys Res Commun
631 205:1438-1444.
632 Giannotti G, Gong S, Fayette N, Heinsbroek JA, Orfila JE, Herson PS, Ford CP, Peters
633 J (2021) Extinction blunts paraventricular thalamic contributions to heroin
634 relapse. Cell Rep 36:109605.
635 Goedecke L, Bengoetxea X, Blaesse P, Pape HC, Jungling K (2019) micro-opioid
636 receptor-mediated downregulation of midline thalamic pathways to basal and
637 central amygdala. Sci Rep 9:17837.
638 Hearing M, Kotecki L, Marron Fernandez de Velasco E, Fajardo-Serrano A, Chung HJ,
639 Lujan R, Wickman K (2013) Repeated cocaine weakens GABA(B)-Girk
640 signaling in layer 5/6 pyramidal neurons in the prelimbic cortex. Neuron
641 80:159-170.
642 Iglesias AG, Flagel SB (2021) The Paraventricular Thalamus as a Critical Node of
643 Motivated Behavior via the Hypothalamic-Thalamic-Striatal Circuit. Front
644 Integr Neurosci 15:706713.
645 Ikeda K, Kobayashi T, Kumanishi T, Niki H, Yano R (2000) Involvement of
646 G-protein-activated inwardly rectifying K (GIRK) channels in opioid-induced
647 analgesia. Neurosci Res 38:113-116.
648 Ikeda K, Kobayashi T, Kumanishi T, Yano R, Sora I, Niki H (2002) Molecular
649 mechanisms of analgesia induced by opioids and ethanol: is the GIRK channel
650 one of the keys? Neurosci Res 44:121-131.
651 Jenab S, Kest B, Franklin SO, Inturrisi CE (1995) Quantitative distribution of the delta
652 opioid receptor mRNA in the mouse and rat CNS. Life Sci 56:2343-2355.
653 Jiang C, Wang X, Le Q, Liu P, Liu C, Wang Z, He G, Zheng P, Wang F, Ma L (2021)
654 Morphine coordinates SST and PV interneurons in the prelimbic cortex to
655 disinhibit pyramidal neurons and enhance reward. Mol Psychiatry
656 26:1178-1193.
657 Jullie D, Stoeber M, Sibarita JB, Zieger HL, Bartol TM, Arttamangkul S, Sejnowski TJ,
658 Hosy E, von Zastrow M (2020) A Discrete Presynaptic Vesicle Cycle for
659 Neuromodulator Receptors. Neuron 105:663-677 e668.

660 Just S, Illing S, Trester-Zedlitz M, Lau EK, Kotowski SJ, Miess E, Mann A, Doll C,
661 Trinidad JC, Burlingame AL, von Zastrow M, Schulz S (2013) Differentiation
662 of opioid drug effects by hierarchical multi-site phosphorylation. Mol
663 Pharmacol 83:633-639.
664 Keyes PC, Adams EL, Chen Z, Bi L, Nachtrab G, Wang VJ, Tessier-Lavigne M, Zhu Y,
665 Chen X (2020) Orchestrating Opiate-Associated Memories in Thalamic
666 Circuits. Neuron 107:1113-1123 e1114.
667 Kieffer BL, Evans CJ (2009) Opioid receptors: from binding sites to visible molecules
668 in vivo. Neuropharmacology 56 Suppl 1:205-212.
669 Kirouac GJ (2015) Placing the paraventricular nucleus of the thalamus within the brain
670 circuits that control behavior. Neurosci Biobehav Rev 56:315-329.
671 Kotecki L, Hearing M, McCall NM, Marron Fernandez de Velasco E, Pravetoni M,
672 Arora D, Victoria NC, Munoz MB, Xia Z, Slesinger PA, Weaver CD, Wickman
673 K (2015) GIRK Channels Modulate Opioid-Induced Motor Activity in a Cell
674 Type- and Subunit-Dependent Manner. J Neurosci 35:7131-7142.
675 Le Merrer J, Becker JA, Befort K, Kieffer BL (2009) Reward processing by the opioid
676 system in the brain. Physiol Rev 89:1379-1412.
677 Luscher C, Slesinger PA (2010) Emerging roles for G protein-gated inwardly rectifying
678 potassium (GIRK) channels in health and disease. Nat Rev Neurosci
679 11:301-315.
680 Mansour A, Fox CA, Burke S, Meng F, Thompson RC, Akil H, Watson SJ (1994) Mu,
681 delta, and kappa opioid receptor mRNA expression in the rat CNS: an in situ
682 hybridization study. J Comp Neurol 350:412-438.
683 Marchant NJ, Furlong TM, McNally GP (2010) Medial dorsal hypothalamus mediates
684 the inhibition of reward seeking after extinction. J Neurosci 30:14102-14115.
685 Marie N, Aguila B, Allouche S (2006) Tracking the opioid receptors on the way of
686 desensitization. Cell Signal 18:1815-1833.
687 McDevitt DS, Graziane NM (2019) Timing of Morphine Administration Differentially
688 Alters Paraventricular Thalamic Neuron Activity. eNeuro 6.
689 Millan EZ, Ong Z, McNally GP (2017) Paraventricular thalamus: Gateway to feeding,
690 appetitive motivation, and drug addiction. Prog Brain Res 235:113-137.
691 Minami M, Satoh M (1995) Molecular biology of the opioid receptors: structures,
692 functions and distributions. Neurosci Res 23:121-145.
693 Nockemann D, Rouault M, Labuz D, Hublitz P, McKnelly K, Reis FC, Stein C,
694 Heppenstall PA (2013) The K(+) channel GIRK2 is both necessary and
695 sufficient for peripheral opioid-mediated analgesia. EMBO Mol Med
696 5:1263-1277.
697 Rifkin RA, Moss SJ, Slesinger PA (2017) G Protein-Gated Potassium Channels: A
698 Link to Drug Addiction. Trends Pharmacol Sci 38:378-392.
699 Wang X, Chou XL, Zhang LI, Tao HW (2020) Zona Incerta: An Integrative Node for
700 Global Behavioral Modulation. Trends Neurosci 43:82-87.

Williams JT, Christie MJ, Manzoni O (2001) Cellular and synaptic adaptations mediating opioid dependence. Physiol Rev 81:299-343.

Williams JT, Ingram SL, Henderson G, Chavkin C, von Zastrow M, Schulz S, Koch T, Evans CJ, Christie MJ (2013) Regulation of mu-opioid receptors: desensitization, phosphorylation, internalization, and tolerance. Pharmacol Rev 65:223-254.

Yousuf A, Miess E, Sianati S, Du YP, Schulz S, Christie MJ (2015) Role of Phosphorylation Sites in Desensitization of micro-Opioid Receptor. Mol Pharmacol 88:825-835.

Zhang X, van den Pol AN (2017) Rapid binge-like eating and body weight gain driven by zona incerta GABA neuron activation. Science 356:853-859.

Zhang Z, Tao W, Hou YY, Wang W, Lu YG, Pan ZZ (2014) Persistent pain facilitates response to morphine reward by downregulation of central amygdala GABAergic function. Neuropsychopharmacology 39:2263-2271.

Zhou K, Zhu Y (2019) The paraventricular thalamic nucleus: A key hub of neural circuits underlying drug addiction. Pharmacol Res 142:70-76.

Zhou K, Zhu L, Hou G, Chen X, Chen B, Yang C, Zhu Y (2021) The Contribution of Thalamic Nuclei in Salience Processing. Front Behav Neurosci 15:634618.

Zhu Y, Wienecke CF, Nachtrab G, Chen X (2016) A thalamic input to the nucleus accumbens mediates opiate dependence. Nature 530:219-222.

Zhu Y, Nachtrab G, Keyes PC, Allen WE, Luo L, Chen X (2018) Dynamic salience processing in paraventricular thalamus gates associative learning. Science 362:423-429.

Figure Legends

Figure 1. Morphine and the MOR agonist DAMGO reduce the firing rate of PVT neurons in brain slices.

A, Immunostaining images showing that saline and morphine i.p. injections induced robust expression of c-Fos (green) in the PVT neurons (n = 2 mice per group). PVT areas are shown in yellow boxes. Scale bar: 500 μm.

B, Normalized density of PVT projection neurons expressing c-Fos. Morphine i.p. injection (blue bar, n = 2 mice) induced more c-Fos positive (c-Fos^{+}) cells in the PVT, compared to saline i.p. injection (gray bar, n = 2 mice) (saline, 101.8 ± 11.57 % vs. morphine, 167.5 ± 13.75 %, P = 0.0016, t = 3.676, df = 19, unpaired t test).

C, Representative recording showing that morphine (30 μM) reduced action potential firing in the PVT, and that the opioid receptor antagonist naloxone (10 μM) reversed this effect.

D, Representative recording showing that the MOR agonist DAMGO (1 μM) reduced action potential firing in the PVT, and the opioid receptor antagonist naloxone (10 μM) reversed this effect.

E, Morphine (30 μM) significantly decreased the firing rate of most PVT neurons (ACSF, 5.06 ± 0.42 Hz, n = 16 vs. morphine, 1.64 ± 0.60 Hz, n = 16 vs. morphine + naloxone, 4.27 ± 0.55 Hz, n = 8. One-way ANOVA, $F_{(1, 16)}$ = 19.63, P = 0.0002, followed by post-hoc Tukey's test). Naloxone was not applied to all the cells.

747 *F*, The MOR agonist DAMGO (1 μM) also significantly decreased the firing rate of
748 most PVT neurons (ACSF, 5.17 ± 0.39 Hz, n = 16 vs. DAMGO, 2.33 ± 0.77 Hz, n =
749 16 vs. DAMGO + naloxone, 3.82 ± 0.30 Hz, n = 12. One-way ANOVA, $F_{(1, 19)}$ =
750 22.04, P < 0.0001, followed by post-hoc Tukey's test). Naloxone was not applied to
751 all the cells.
752 *G*, The KOR agonist U50488 (1 μM) didn't change the firing rate of PVT neurons
753 (ACSF, 5.92 ± 0.54 Hz vs. U50488, 6.31 ± 0.59 Hz, n = 10, P = 0.4278, t = 0.83, df =
754 9, paired t test).
755 *H*, DOR agonist SNC80 (3 μM) did not change the firing rate of PVT neurons (ACSF,
756 6.13 ± 0.61 Hz vs. 5.63 ± 0.60 Hz, n = 10, P = 0.1679, t = 1.5, df = 9, paired t test).
757 *I*, Examples of PVT neuron morphology with Lucifer yellow staining. Scale bar: 50
758 μm.
759 *J*, Schematic of single-cell real-time PCR to test the gene *oprm1* expression of the
760 μ-opioid receptor in the PVT. GAPDH was used as an internal control.
761 *P < 0.05, **P < 0.01, ***P < 0.001, N.S.: nonsignificance.
762

Figure 2. Effects of morphine on spontaneous excitatory and inhibitory inputs to PVT neurons.

A, Example traces showing spontaneous excitatory postsynaptic currents (EPSCs) before (black) and after (red) morphine (30 μM) application in brain slices.

B and C, No differences were found in the amplitude and frequency of spontaneous EPSCs before and after morphine (30 μM) application (Amplitude: ACSF, 11.09 ± 0.72 pA vs. morphine, 10.45 ± 0.56 pA, n = 14, P = 0.444, t = 0.79, df = 13; Frequency: ACSF, 4.94 ± 0.59 vs. morphine, 4.53 ± 0.53 Hz, n = 14, P = 0.1824, t = 1.41, df = 13, paired t test).

D, Example traces showing spontaneous inhibitory postsynaptic currents (IPSCs) before (black) and after (blue) morphine (30 μM) application in brain slices.

E and F, Morphine (30 μM) reduced the amplitude and frequency of spontaneous IPSCs (Amplitude: ACSF, 13.30 ± 0.91 pA vs. morphine, 11.89 ± 0.66 pA, n = 18, P = 0.0078, t = 3.01, df = 17; Frequency: ACSF, 4.03 ± 0.90 vs. morphine, 3.31 ± 0.68 Hz, n = 18, P = 0.0133, t = 2.76, df = 17, paired t test).

*P < 0.05, **P < 0.01, N.S.: nonsignificance.

Figure 3. Activation of opioid receptors reduces the inhibitory transmission of PVT neurons.

A, Example traces showing the miniature inhibitory postsynaptic currents (mIPSCs) before (black) and after (blue) morphine (30 μM) application. mIPSCs were recorded in the presence of APV (50 μM), CNQX (10 μM) and TTX (0.5 μM).

B, Morphine (30 μM) reduced the amplitude (left) and frequency (right) of mIPSCs (Amplitude: ACSF, 8.32 ± 0.54 pA vs. morphine, 7.52 ± 0.54 pA, n = 10, P = 0.0015, t = 4.48, df = 9; Frequency: ACSF, 2.88 ± 0.31 Hz vs. morphine, 2.34 ± 0.33 Hz, n = 10, P = 0.0028, t = 4.07, df = 9, paired t test).

C, Example traces showing the mIPSCs before (black) and after (red) the application of the MOR agonist DAMGO (1 μM).

D, DAMGO (1 μM) reduced the amplitude (left) and frequency (right) of mIPSCs (Amplitude: ACSF, 9.57 ± 0.85 pA vs. DAMGO, 8.71 ± 0.75 pA, n = 12, P = 0.0353, t = 2.4, df = 11; Frequency: ACSF, 2.66 ± 0.38 Hz vs. DAMGO, 2.04 ± 0.41 Hz, n = 12, P = 0.0006, t = 4.73, df = 11, paired t test).

E, Example traces showing the mIPSCs before (black) and after (green) application of the KOR agonist U50488 (1 μM).

F, U50488 (1 μM) also reduced the amplitude (left) and frequency (right) of mIPSCs (Amplitude: ACSF, 11.48 ± 0.75 pA vs. U50488, 10.02 ± 0.64 pA, n = 12, P = 0.0005, t = 4.9, df = 11; Frequency: ACSF, 4.35 ± 0.97 Hz vs. U50488, 3.11 ± 0.70 Hz, n = 12, P = 0.0014, t = 4.26, df = 11, paired t test).

G, Example traces showing the mIPSCs before (black) and after (purple) application of the DOR agonist SNC80 (3 μM).

H, No differences were found after SNC80 (3 μM) application (Amplitude: ACSF, 13.94 ± 1.07 pA vs. SNC80, 13.42 ± 1.01 pA, n = 12, P = 0.0965, t = 1.82, df = 11; Frequency: ACSF, 4.95 ± 0.64 Hz vs. SNC80, 4.75 ± 0.51 Hz, n = 12, P = 0.4612, t = 0.76, df = 11, paired t test).

*P < 0.05, **P < 0.01, ***P < 0.001, N.S.: nonsignificance.

Figure 4. The KOR agonist U50488 reduces inhibitory synaptic transmission from the ZI to the PVT.

A, Schematic illustration of the viral approach for retrograde tracing used in GAD2-Cre transgenic mice.

B, Representative image of retrograde tracing and EGFP expression in the upstream regions (green). Scale bar: 2 mm (upper panels), 500 μm (lower panels). SCN: suprachiasmatic nucleus, ZI: zona incerta, cRt: caudal reticular thalamus, DR: dorsal raphe.

C, Schematic illustration of the optogenetic approach used to test synaptic transmission from the ZI to the PVT.

D, Example traces of optically evoked IPSCs (oIPSCs) induced by a single light pulse (470 nm, 2 ms), and PVT neurons recorded when holding approximately 0 mV. No current was evoked when held at -70 mV (upper). These oIPSCs could be blocked by the $GABA_A$ receptor antagonist picrotoxin (100 μM) (lower).

E, Example traces of oIPSCs induced by a single light pulse (470 nm, 2 ms) before (upper) and after (lower) TTX (1 μM) and 4-AP (1 mM) application.

F, The amplitude of oIPSCs is not changed by TTX (1 μM) and 4-AP (1 mM) in PVT neurons (ACSF, 339.0 ± 74.10 pA vs. TTX + 4-AP, 344.2 ± 54.05 pA, n = 8, P = 0.8725, t = 0.17, df = 7, paired t test).

G, Example traces showing the oIPSCs before and after DAMGO (1 μM) (upper) and U50488 (1 μM) application (lower).

H and I, The amplitude and paired-pulse ratio (PPR) of oIPSCs were not different before and after DAMGO (1 μM) application (Amplitude: ACSF, 164.7 ± 34.95 pA vs. DAMGO, 185.0 ± 42.65 pA, n = 13, P = 0.2109, t = 1.32, df = 12; PPR: ACSF, 1.02 ± 0.08 vs. DAMGO, 1.01 ± 0.071, n = 13, P = 0.861, t = 0.18, df = 12, paired t test). The PPR was elicited by two consecutive light pulses (470 nm, 2 ms) with an interval of 100 ms.

J and K, The amplitude of oIPSCs was reduced after U50488 (1 μM) application, but there was no difference for the paired-pulse ratio (Amplitude: ACSF, 134.0 ± 21.08 pA vs. U50488, 105.3 ± 20.16 pA, n = 11, P = 0.0123, t = 3.05, df = 10; PPR: ACSF, 1.02 ± 0.05 vs. U50488, 1.12 ± 0.12, n = 11, P = 0.3107, t = 1.07, df = 10, paired t test).

*P < 0.05, N.S.: nonsignificance.

Figure 5. Chronic morphine treatment attenuates the inhibitory effects of DAMGO on the firing rate of PVT neurons, which is partly mediated by GIRK channels.

A, Experimental schedule for chronic morphine treatment: morphine i.p. injection for 5 consecutive days with a concentration gradient. Patch clamp recording on day 7.

B, Action potential firings were recorded in the PVT after chronic saline treatment, and DAMGO (1 μM) significantly reduced the firing rate in saline-treated mice (ACSF, 2.91 ± 0.33 Hz vs. DAMGO, 0.64 ± 0.34 Hz vs. DAMGO + Naloxone, 2.53 ± 0.37 Hz; n = 12. One-way ANOVA, $F_{(1, 14)} = 22.93$, P = 0.0001, followed by post-hoc Tukey's test).

C, Action potential firings were recorded in the PVT after chronic morphine treatment, and the reduction in firing rate was attenuated compared to that in saline-treated mice (ACSF, 4.79 ± 0.36 Hz vs. DAMGO, 3.66 ± 0.61 Hz vs. DAMGO + Naloxone, 4.73 ± 0.34 Hz; n = 15. One-way ANOVA, $F_{(1, 18)} = 5.998$, P = 0.0184, followed by post-hoc Tukey's test).

D, Representative recording showing that DAMGO (1 μM) reduced action potential firing in the PVT of the saline-treated mice, and that naloxone (10 μM) reversed this effect.

E, Representative recording showing that DAMGO (1 μM) could not significantly reduce firing in the morphine-treated mice.

F, Experimental schedule for morphine exposure: morphine i.p. injection for 5 consecutive days with a concentration gradient. Two hours after the injection on day 5, the mouse was anesthetized and decapitated for preparation of brain slices.

G, Experimental schedule for naloxone-precipitated withdrawal: morphine i.p. injection for 5 consecutive days with a concentration gradient. Two hours after the injection on day 5, the mouse was i.p. injected with naloxone (5 mg/kg). 10-15 min later, the mouse was anesthetized and decapitated for preparation of brain slices.

H, Action potential firings were recorded in the PVT of morphine exposed mice. DAMGO (1 μM) did not significantly reduce the firing rates (ACSF, 3.03 ± 0.25 Hz vs. DAMGO, 2.25 ± 0.44 Hz vs. DAMGO + Naloxone, 2.91 ±0.22 Hz; n = 9. One-way ANOVA, $F_{(1, 12)} = 2.339$, P = 0.1472, followed by post-hoc Tukey's test).

I, Action potential firings were recorded in the PVT of naloxone-precipitated withdrawal mice. DAMGO (1 μM) could not significantly reduce the firing rates, which is similar to that in morphine-treated mice (ACSF, 3.59 ± 0.33 Hz vs. DAMGO, 2.71 ± 0.56 Hz vs. DAMGO + Naloxone, 3.73 ±0.30 Hz; n = 6. One-way ANOVA, $F_{(1, 6)} = 6.134$, P = 0.0466, followed by post-hoc Tukey's test).

J, Suppression ratio for firing in the saline-treated, morphine-treated, morphine exposure and naloxone-precipitated withdrawal groups. Percentage of change in the firing rate was calculated by dividing the data in drug divided by that in ACSF (saline treatment, 0.18 ± 0.09, n = 12 vs. morphine treatment, 0.74 ± 0.10, n = 15 vs. morphine exposure, 0.75 ± 0.12, n = 9 vs. naloxone-precipitated withdrawal, 0.74 ±

884 0.13, n = 6. One-way ANOVA, $F_{(2, 14)}$ = 7.797, P = 0.0063, followed by post-hoc
885 Dunnett's test).
886 *K*, Example traces of GIRK currents induced by DAMGO (3 μM) in the saline-treated
887 mice (black), morphine-treated mice (red), morphine-exposed mice (blue) and
888 naloxone-precipitated withdrawal mice (orange). U50488 (3 μM) could not induce
889 GIRK currents in the saline-treated mice (green).
890 *L*, There was no difference in the GIRK currents between the saline-treated and
891 morphine-treated mice, and no difference between the saline-treated and
892 morphine-exposed mice. The GIRK currents were much smaller in the
893 naloxone-precipitated withdrawal mice than that in the saline-treated mice (saline
894 treatment, 19.09 ± 4.03 pA, n = 9 vs. morphine treatment, 22.67 ± 3.29 pA, n = 11 vs.
895 morphine exposure, 15.32 ± 4.45 pA, n = 7 vs. naloxone-precipitated withdrawal,
896 2.82 ± 1.96 pA, n = 6. One-way ANOVA, $F_{(2, 16)}$ = 4.714, P = 0.0288, followed by
897 post-hoc Dunnett's test).
898 *M*, Example recording showing that DAMGO (1 μM) hyperpolarized the membrane
899 potential and abolished firing, but the GIRK channel antagonist tertiapin-Q (1 μM)
900 could not fully reverse this effect in wild-type mice.
901 *N*, Tertiapin-Q (1 μM) could not reverse the firing rates (ACSF, 3.28 ± 0.33 Hz vs.
902 DAMGO, 0.18 ± 0.18 Hz vs. DAMGO + Tertiapin-Q, 0.60 ± 0.56 Hz, n = 5.
903 One-way ANOVA, $F_{(1, 5)}$ = 27.05, P = 0.0028, followed by post-hoc Tukey's test).

O, DAMGO (1 μM) significantly decreased the membrane potential, but the GIRK channel antagonist Tertiapin-Q (1 μM) could not fully reverse it (ACSF, -40.29 ± 1.93 mV vs. DAMGO, -49.27 ± 2.22 mV vs. DAMGO + Tertiapin-Q, -43.39 ± 1.11 mV, n = 5. One-way ANOVA, $F_{(1, 6)} = 11.82$, P = 0.0118, followed by post-hoc Tukey's test).

*P < 0.05, **P < 0.01, ***P <0.001, N.S.: nonsignificance.

Figure 6. Chronic morphine exposure causes MOR internalization.

A, Confocal images showing the distribution of MOR (red) in the cell bodies of the PVT after chronic saline and morphine treatment. NeuN antibody was used to visualize the cell body (green). Scale bar: 5 μm.

B, Radius analysis showing the distribution of MOR from the center to the periphery of the PVT cells (n = 8 per group). MORs were scattered in the cell body (cytoplasm) in the chronic morphine group (red line), and MORs were mostly distributed in the periphery (membrane) in the saline group (black line).

C, Quantification analysis shows that more MORs were distributed in the cytoplasm in the PVT cells of morphine-treated mice, corresponding to the blue box in B (morphine treatment, 47.67 ± 1.78 vs. saline treatment, 36.39 ± 1.18, n = 8). More MORs were distributed in the membrane area in the PVT cells of saline-treated mice, corresponding to the green box in B (morphine treatment, 45.94 ± 0.43 vs. saline treatment, 67.80 ± 0.73, n = 8). Two-way ANOVA followed by post-hoc Tukey's test; drug treatment × cellular location, $F_{(1, 8)} = 181.7$, $P < 0.0001$; drug treatment, $F_{(1, 8)} = 24.9$, $P < 0.01$; cellular location, $F_{(1, 8)} = 145.8$, $P < 0.0001$. ****P< 0.0001.

Figure 7. Chronic morphine exposure attenuates the suppressive effects of MOR and KOR agonists on inhibitory inputs to PVT neurons, and also reduces the kappa opioid regulation in the ZI to PVT pathway.

A, Example traces showing the mIPSCs before (black) and after (blue) the application of the MOR agonist DAMGO (1 μM) in the saline-treated mice.

B, Example traces showing the mIPSCs before (black) and after (green) KOR agonist U50488 (1 μM) application in the saline-treated mice.

C and D, DAMGO (1 μM) reduced the amplitude and frequency of mIPSCs in saline-treated mice (Amplitude: ACSF, 9.01 ± 0.82 pA vs. DAMGO, 8.55 ± 0.82 pA, n = 11, P = 0.0459, t = 2.28, df = 10; Frequency: ACSF, 3.76 ± 0.85 Hz vs. DAMGO, 3.52 ± 0.83 Hz, n = 11, P = 0.006, t = 3.47, df = 10, paired t test).

E and F, U50488 (1 μM) reduced the amplitude and frequency of mIPSCs in saline-treated mice (Amplitude: ACSF, 8.30 ± 0.44 pA vs. U50488, 7.44 ± 0.40 pA, n = 13, P = 0.0013, t = 4.19, df = 12; Frequency: ACSF, 4.01 ± 0.56 Hz vs. U50488, 3.01 ± 0.44 Hz, n = 13, P = 0.0077, t = 3.19, df = 12, paired t test).

G, Example traces showing the mIPSCs before (black) and after (red) DAMGO (1 μM) application in the morphine-treated mice.

H, Example traces showing the mIPSCs before (black) and after (purple) U50488 (1 μM) application in the morphine-treated mice.

I and J, DAMGO (1 μM) failed to alter the amplitude and frequency of mIPSCs after chronic morphine treatment (Amplitude: ACSF, 9.66 ± 0.79 pA vs. DAMGO, 9.11 ±

0.66 pA, n = 12, P = 0.0794, t = 1.93, df = 11; Frequency: ACSF, 4.33 ± 0.78 Hz vs. DAMGO, 3.81 ± 0.72 Hz, n = 12, P = 0.0544, t = 2.15, df = 11, paired t test).

K and L, U50488 (1 μM) could not change the amplitude of mIPSCs after chronic morphine treatment (ACSF, 8.31 ± 0.86 pA vs. U50488, 8.05 ± 0.80 pA, n = 12, P = 0.266, t = 1.17, df = 11, paired t test). U50488 (1 μM) reduced the frequency of mIPSCs (ACSF, 2.94 ± 0.56 Hz vs. U50488, 2.63 ± 0.54 Hz, n = 12, P = 0.0495, t = 2.21, df = 11, paired t test), but the effects were attenuated in morphine-treated mice compared to saline-treated mice.

M, The amplitude of oIPSCs was reduced after U50488 (1 μM) application in the saline-treated mice, but the paired-pulse ratio did not change (Amplitude: ACSF, 255.3 ± 21.94 pA vs. U50488, 205.9 ± 19.36 pA, n = 20, P = 0.00007, t = 5.06, df = 19; PPR: ACSF, 0.91 ± 0.04 pA vs. U50488, 0.91 ± 0.03 pA, n = 20, P = 0.7451, t = 0.33, df = 19, paired t test).

N, The amplitude and the paired-pulse ratio (PPR) of oIPSCs didn't change after U50488 (1 μM) application in the morphine-treated mice (Amplitude: ACSF, 108.2 ± 13.85 pA vs. U50488, 103.2 ± 14.03 pA, n = 19, P = 0.2403, t = 1.21, df = 18; PPR: ACSF, 1.08 ± 0.12 pA vs. U50488, 1.19 ± 0.13 pA, n = 14, P = 0.196, t = 1.36, df = 13, paired t test).

*P < 0.05, **P < 0.01, ****P <0.0001, N.S.: nonsignificance.

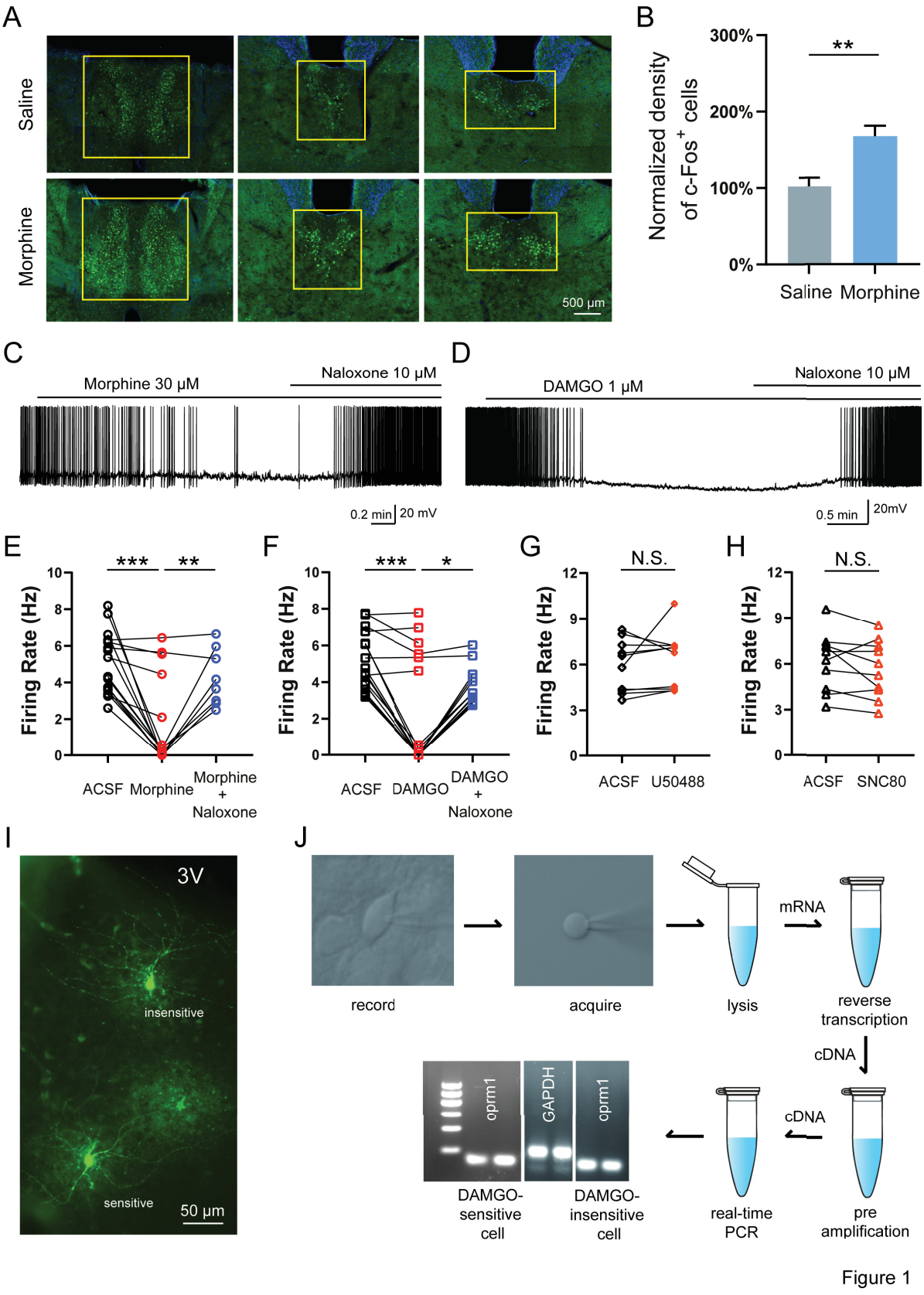

Figure 1

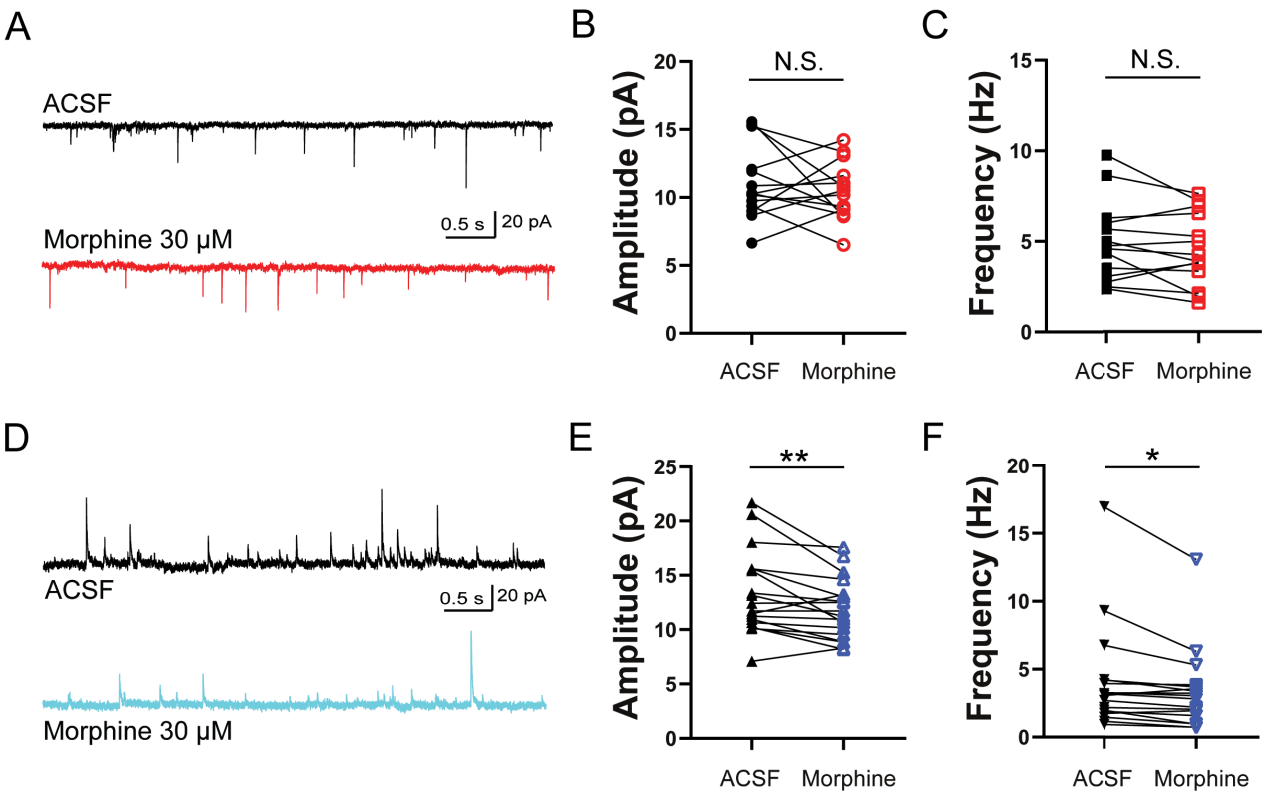

Figure 2

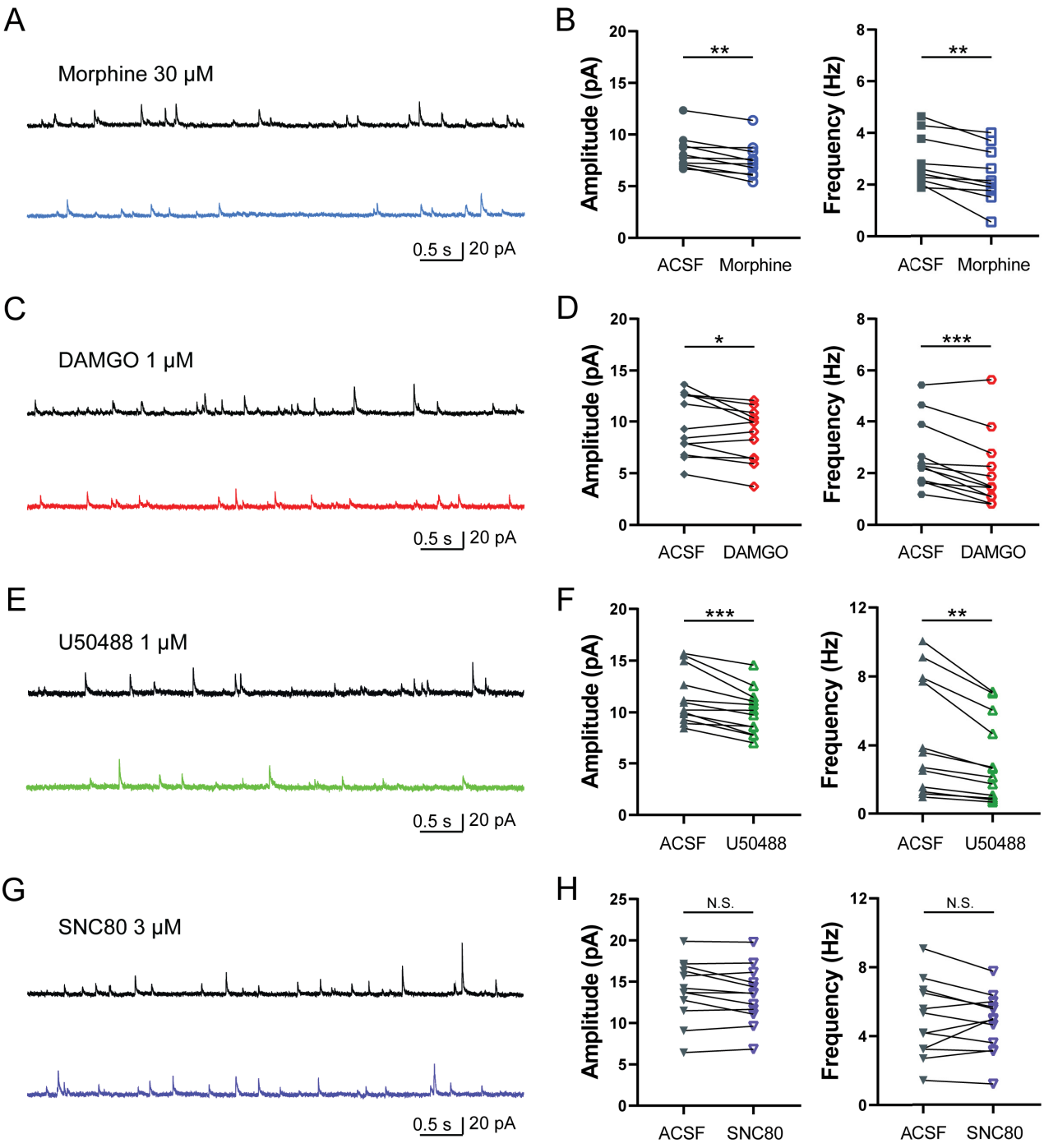

Figure 3

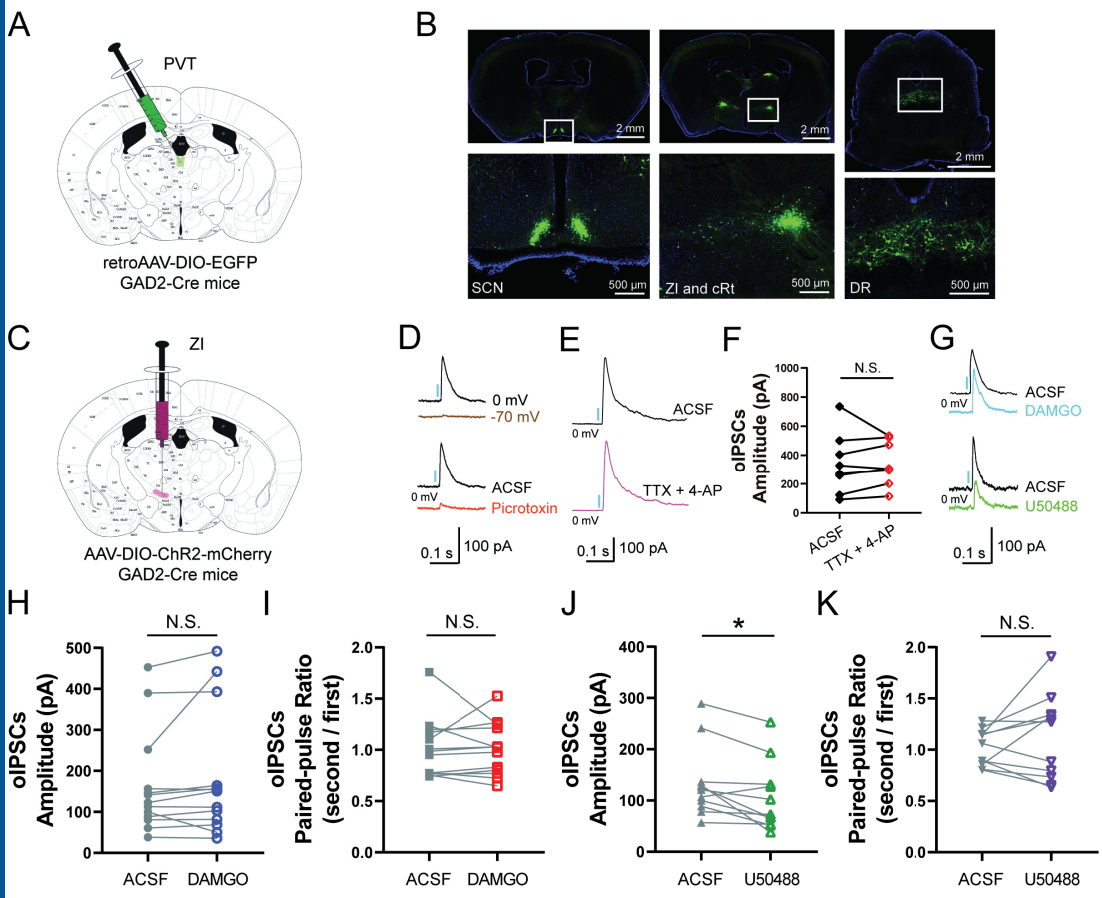

Figure 4

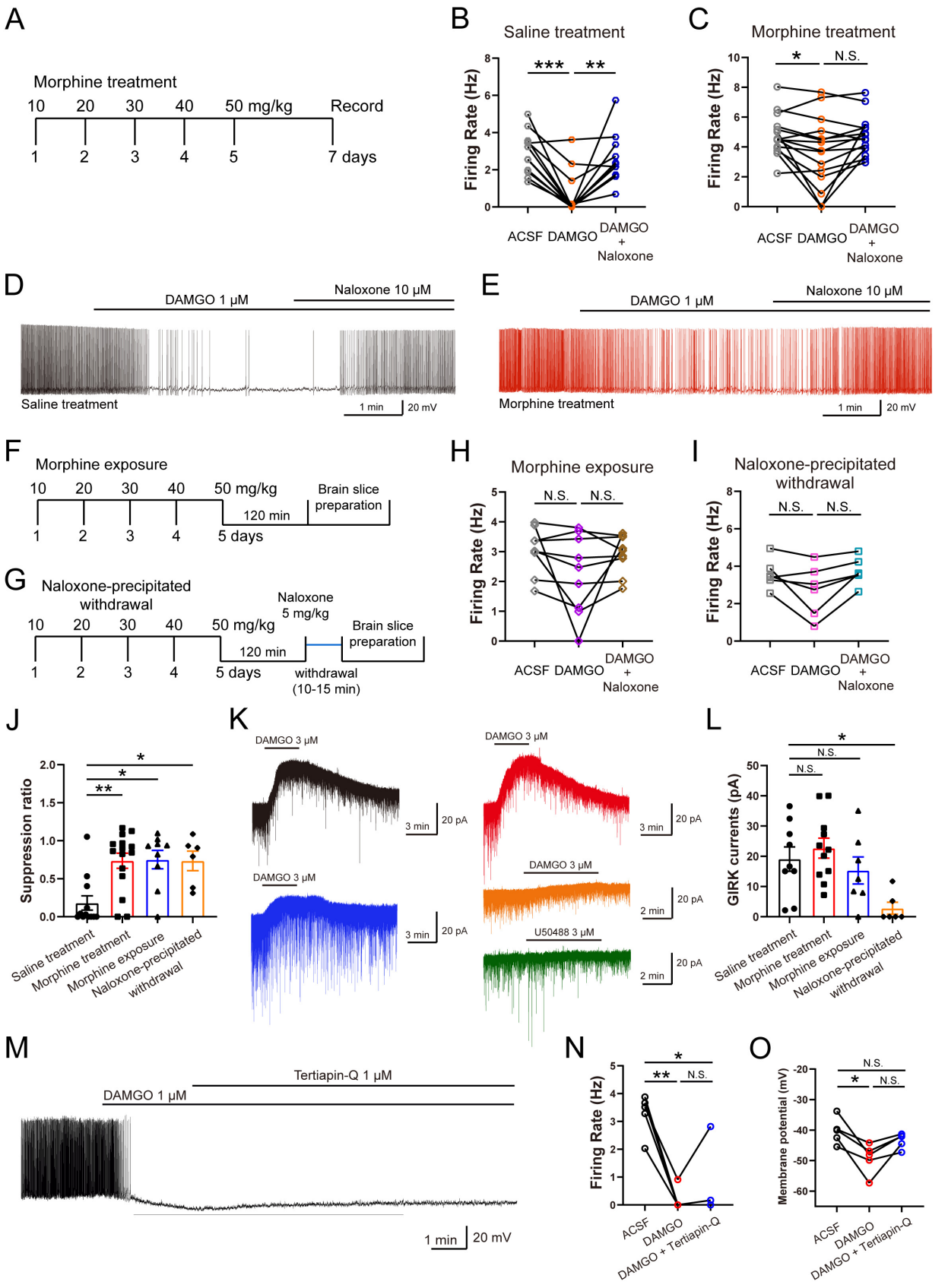

Figure 5

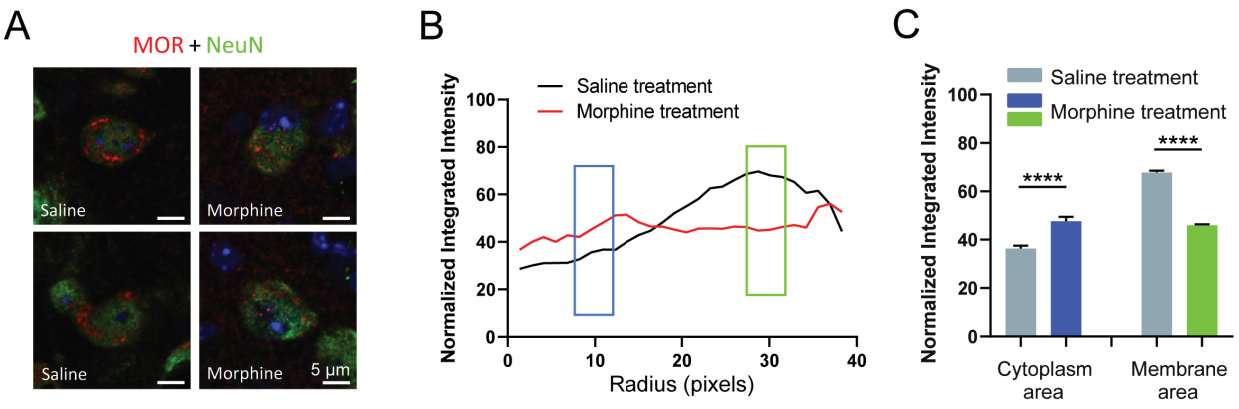

Figure 6

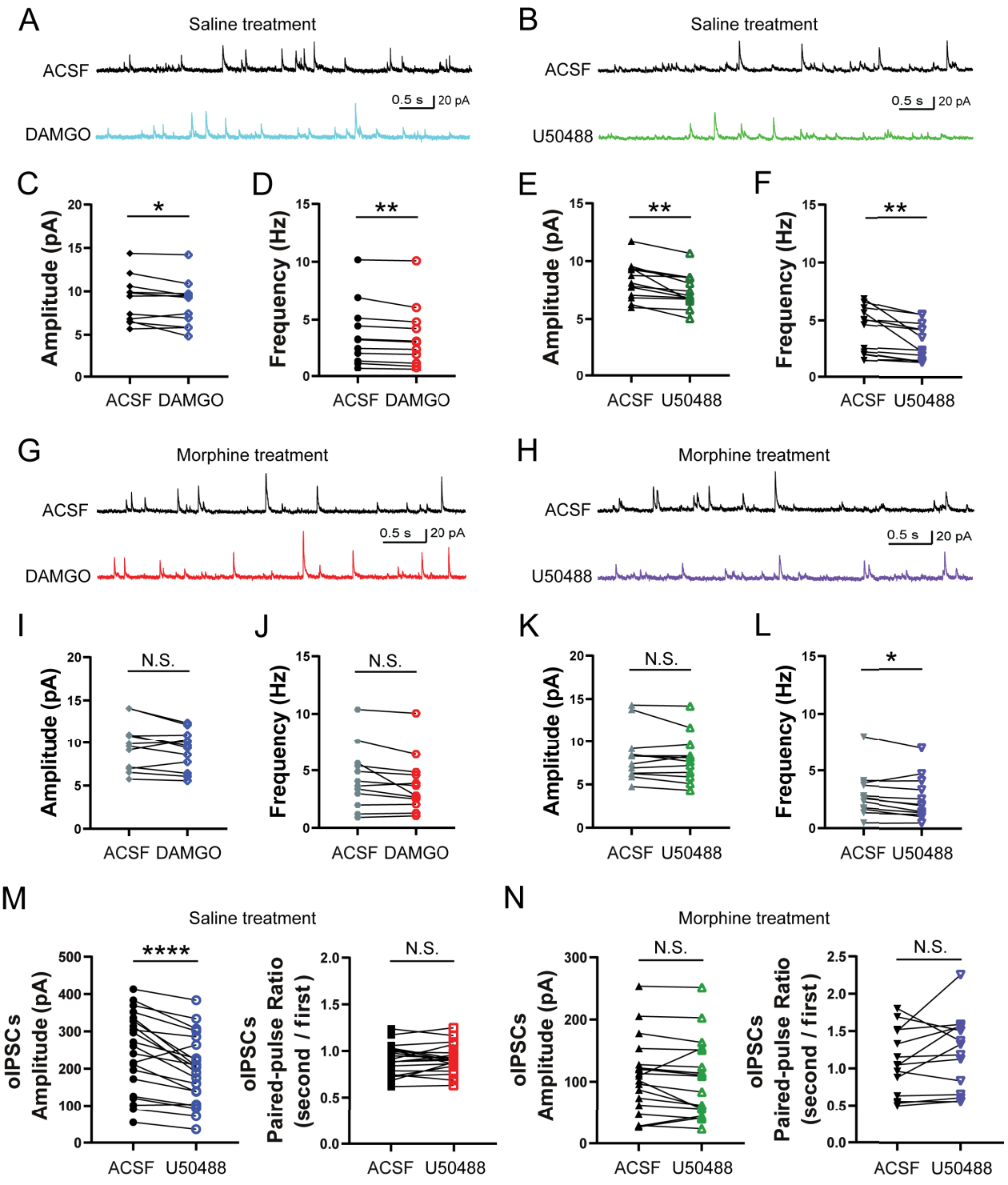

Figure 7